Stability of parallel flows in a microchannel after a T junction

Pierre Guillot* and Annie Colin
Rhodia Laboratoire du Futur, Unité mixte Rhodia-CNRS, Université Bordeaux I, 178 Avenue Schweitzer, 33608 Pessac, France
(Received 22 March 2005; published 5 December 2005)

In this work, the flow of immiscible fluids in microchannels is studied. Flow pattern diagrams obtained in microfluidic chips are presented. Monodisperse droplets or parallel flows are obtained depending on the flow rate values of the aqueous phase and the oil phase. Transition from droplet regime to parallel flows cannot be described in terms of capillary numbers. Using confocal microscopy and high speed imaging, it was shown that droplets are formed through a blocking-pinching mechanism ruled by flow rate conservation. Conditions for parallel flow stability are quantified.

DOI: 10.1103/PhysRevE.72.066301 PACS number(s): 47.15.−x, 83.50.Ha, 47.85.Np

Biotechnology, analytical chemistry, and combinatorial chemistry are among the most rapidly evolving disciplines in modern technology. Microfluidics, which deal with the methods and materials to control and handle liquid flows in length scales ranging between tens to hundreds of microns, offers numerous perspectives in these fields of research. In fact, it was shown that scaling down the typical length scales and the amount of handled material, can greatly increase efficiency and reduce the cost of research and development [1]. In microchannels, multiphase flows such as droplets [2], pearls, or parallel flows [3,4] could be a less costly complement to stopped flow methods for a broad range of time-resolved assays in chemistry and biochemistry. For example, droplets can be used as micro reactors to extract kinetic parameters of a chemical reaction [5] or to perform protein crystallization [6]. Parallel flows correspond to fluids flowing continuously side by side and are a way to perform solvent extractions or purifications which are key operations in an analytical processing [7,8]. However, these approaches require strategies to control the stability of the immiscible phase flows. Ismagilov and coworkers [9] have shown that droplet formation after a T junction may be rationalized in terms of capillary numbers. However, the threshold capillary numbers seem to vary as a function of the viscosity contrast between the two phases. This would not be the case if the droplet formation was the result of a competition between the viscous stresses associated with the imposed flow field and the capillary stresses due to surface tension between the two phases [10]. Therefore, at this stage, the mechanism of droplet formation after a T junction in microchannels or the stability of parallel flow remains unclear.

In this paper, a comprehensive study of immiscible fluids flowing after a T junction is performed. Flow pattern diagrams obtained for various channel aspect ratios and various viscosities are presented. The major focus of this work lies in the determination of the shape of the parallel flows by confocal fluorescence microscopy and in the analysis of the droplet formation mechanism. Strikingly, this mechanism does not involve a competition between the viscous forces and the capillary forces, but is captured in terms of a blocking-pinching mechanism. Using a simple model, the conditions required to obtain parallel flow stability are quantified.

Our microfluidic devices are fabricated using soft lithography technology [11]. Poly-dimethyl siloxane (PDMS) channels or PDMS-glass channels are used. The microdevices have two inlet arms which meet at a T junction with a funnel design. The flow patterns are observed in the outlet channel after the T junction. The inlet channels are connected via tubing to syringes loaded with the fluids. Syringe pumps allow control of the flow rates of the liquids. In this study, the immiscible fluids used are aqueous and oil solutions. Oils are silicone oils (Rhodorsil) of different viscosities and hexadecane (Prolabo). Aqueous solutions are dilute solutions of Sodium Dodecyl Sulphate (SDS) (Merck) above the critical micellar concentration (CMC) in water (CMC =0.24 wt %) or in a mixture of glycerine (Prolabo) and water. Adding glycerine allows us to match the optical index of the aqueous solution with silicone oil and thus, enables us to perform fluorescent confocal microscopy.

Figure 1 shows the flow pattern diagram obtained with a mixture of 50 wt % of water with SDS at 2 CMC and

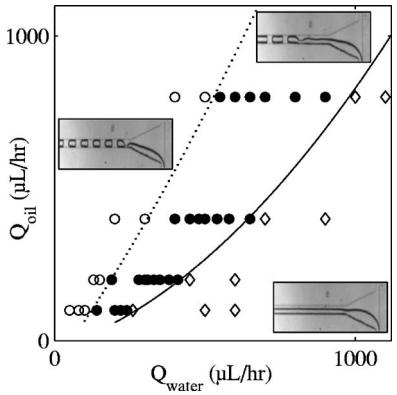

FIG. 1. Flow pattern diagram as a function of the aqueous phase flow rate (Q_{water}) and of the oil phase flow rate (Q_{oil}) in a 100 μm × 100 μm microchannel. The aqueous phase is a mixture of water with SDS (2 CMC) 50 wt % and of glycerine 50 wt %. The oil phase is hexadecane. The ○ refer to droplets formed at the T junction (DTJ), the ◇ to parallel flows (PF), and the ● to parallel flows that break into droplets inside the channel (DC).

*Corresponding author: pierre.guillot-exterieur@eu.rhodia.com

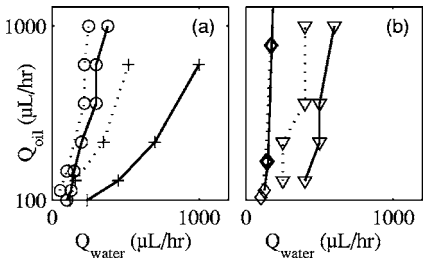

FIG. 2. The aqueous phase is a mixture of water with SDS (2 CMC) 50 wt % and glycerine 50 wt %. The thick lines correspond to the transition between DC and PF and the dotted lines to the transition between DTJ and DC. (a) Effect of the aspect ratio of the microchannel. The oil phase is hexadecane. The + refers to a 100 μm $\times$ 100 μm channel and the ○ to a 200 μm wide $\times$ 100 μm high channel. (b) Effect of the viscosity of the oil phase in a 100 μm $\times$ 100 μm microchannel. The ▽ refers to a 20 cP silicone oil and the ◇ to a 100 cP silicone oil.

50 wt % of glycerine as aqueous phase and hexadecane in a 100 μm $\times$ 100 μm microchannel. The viscosity of the aqueous phase is 7 cP and the oil phase of 3 cP. During the experiment, three typical flow patterns have been identified: droplets formed at the T junction (DTJ), parallel flows (PF), and parallel flows which break into droplets inside the channel (DC). Droplets are obtained in the upper left corner of Fig. 1, i.e., at low water flow rates and substantial oil flow rates. Two kinds of regimes must be distinguished. In the DTJ regime represented by (○), droplets are not always produced with reproducibilty in size, whereas in the DC regime (●), monodisperse droplets are produced. In the latter case, a parallel flow takes place at the entrance of the channel and becomes unstable after a short distance, breaking up into droplets. In the lower right corner, PF are observed. Similar behavior was obtained by Ismagilov in a T junction without a funnel [9].

This diagram depends on the aspect ratio of the cross section and on the oil viscosity (see Fig. 2). Rectangular sections and high oil viscosity favor PF formation and decrease the DC range.

To investigate the three-dimensional structure of the flow, confocal fluorescence microscopy experiments are performed. In this case, rhodamine (Sigma Aldrich) is added to the aqueous phase and hexadecane is used as the oil phase.

Figure 3 displays cross section images obtained for PF in a 100 μm $\times$ 100 μm microchannel. The channel walls represented here have been drawn and added to the picture. The

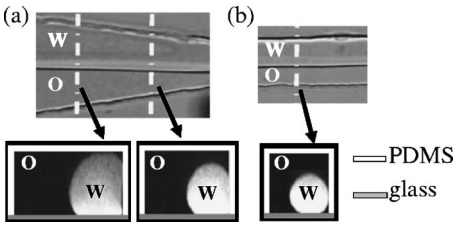

FIG. 3. Cross section picture of parallel flow between hexadecane (O) and aqueous phase with rhodamine (W) in a 100 μm $\times$ 100 μm microchannel. (a) Inside the funnel. (b) In the outlet channel.

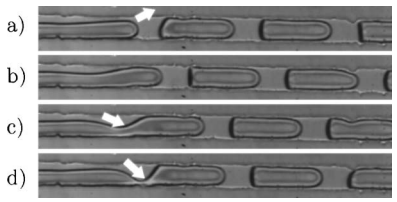

FIG. 4. Droplet formation mechanism in a channel. Example with hexadecane at 900 μL/h and water with SDS at 1200 μL/h in a 100 μm $\times$ 100 μm channel. (a) The tip of the jet begins to expand in the channel, (b) the tip clogs the channel, (c) oil phase starts pinching the water jet, and (d) just before the drop formation. Time period is 3.1 ms.

bottom wall is in glass and the three others are in PDMS. At the entrance of the funnel, hexadecane starts wrapping around the water. This is due to the difference of wettability of the two fluids with the PDMS walls. The water flow cross section continues evolving until the flow mainly evolves along the propagation axis. Depending on the flow rates, PF or DC are then observed. PF is a truncated cylinder jet located on the glass at the PDMS glass corner. The pressure in a cross section is uniform inside each fluid and differs from one fluid to the other. The Laplace law imposes that the free fluid surface has a single curvature radius.

Figure 4 shows the DC formation mechanism. The tip advances in the microchannel by expanding in size. It stops growing when it hits the channel walls. The water acts as a plug blocking the oil. The oil phase pinches the jet. This produces the breaking of the PF and the formation of droplets. Let us focus on the tip of the cylindar jet. In contrast to the cylinder part of the jet, which has a single radius of curvature, R_{cylinder}, the tip has two radii of curvature, R_1 and R_2. The pressure jump between the two phases evolves from $\Gamma/R_{\text{cylinder}}$ in the cylinder to $\Gamma/(R_1+R_2)$ in the tip, where Γ is the interfacial tension. This leads to a pressure gradient perpendicular to the propagation axis of the channel and gives rise to a perpendicular flow. The growing of the tip relaxes the stress by increasing the curvature radius and decreasing the Laplace pressure. The cross section S of the tip is a single radius shape respecting the wetting conditions on the glass (partial wetting) and on the PDMS (nonwetting) and minimizing the pressure drop in the tip.

The mechanism of DC formation is nonintuitive since it cannot be described in terms of a competition between viscous and capillary forces, as it is for droplet fragmentation at a T junction [12]. The capillary numbers [i.e., the ratio of the viscous forces by the interfacial forces ($\text{Ca}=\eta\dot{\gamma}R/\Gamma$)] have been plotted as a function of the water flow rate in Fig. 5. η is the viscosity of the oil phase, $\dot{\gamma}$ is the mean shear rate at the interface, and R is the radius of the curvature. In order to estimate $\dot{\gamma}$, the flow field inside the channel has been computed by solving the Stokes equation. The following assumptions have been made: the velocity field is born by the propagation axis, no slipping occurs at the walls of the channels, and the stress tensor and the velocity are continuous at the interface between the two fluids. The water phase is a jet in which radius R is measured on the optical picture, the contact angle between water and glass plate θ does not vary as a

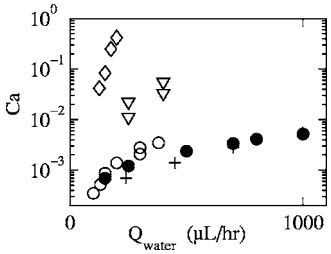

FIG. 5. Capillary number at the transition DC-PF as a function of the water flow rate. ● corresponds to the SDS solution in water at CMC with hexadecane in a 100 μm × 200 μm PDMS microchannel. +, ▽, and ◇ are obtained in a 100 μm × 100 μm PDMS-glass channel with water glycerine and hexadecane for +, 20 cP silicone oil for ▽, and 100 cP silicone oil for ◇. ○ corresponds to a water-glycerine solution with hexadecane in a 200 μm wide × 100 μm high PDMS-glass channel.

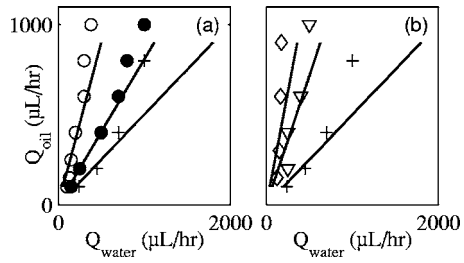

FIG. 7. Lines correspond to theoretical DC-PF transition. ● correspond to SDS solution in water at CMC with hexadecane in a 100 μm × 200 μm PDMS microchannel. +, ▽, and ◇ are obtained in a 100 μm × 100 μm PDMS-glass channel with water, glycerine, and hexadecane for +, 20 cP silicone oil for ▽ and 100 cP silicone oil for ◇. ○ corresponds, to water glycerine solution with hexadecane in a 200 μm wide × 100 μm high PDMS-glass channel. $\theta = 45°$ for glass-PDMS channel and $\theta = 0°$ for PDMS channel.

function of the flow rates and is measured on the confocal pictures. Clearly, Fig. 5 shows that the capillary numbers Ca are less than one at the transition and that no particular value of this parameter is met at the transition. Moreover, for a given Q_{water}, increasing the viscosity of the continuous phase increases the capillary number but promotes the PF (see ▽ and ◇ in Fig. 5). Breaking of the droplets is thus not controlled by a competition between viscous forces and capillary forces. Viscous forces are too low to deform the jet. Similar behavior was previously observed in a gas-liquid system [13,14], where the capillary numbers were calculated roughly using the dimensional relationship $\mathrm{Ca} = \eta Q_{oil}/\Gamma S$. Note that applying this relation to our data do not significantly modify Fig. 5. Figure 6 shows a cross section inside the jet and tip before pinching. In the following, a model based on the blocking-pinching effect is developed.

In the system of reference of the tip, the conservation of the oil phase requires the incoming volume of oil arriving from the entrance of the channel to be equal to the outgoing volume of oil going out, plus the volume of oil remaining trapped behind the tip Ω. After a time T, the amount of liquid blocked behind the tip is equal to

$$\Omega = T\left(\frac{Q_{\mathrm{oil}}}{S_c - s} - V_t\right)(S_c - s) - T(V_o - V_t)(S_c - S), \qquad (1)$$

where V_t is the tip velocity, V_o is the oil velocity in the vicinity of the tip, S_c is the cross section area of the channel, s the cross section area of the jet before the tip, and S the cross section area of the tip. In the following, it will be assumed that the PF will be unstable when the volume Ω is positive. This criterion will be used to calculate a theoretical

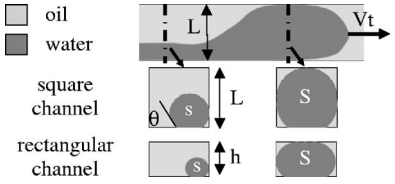

FIG. 6. Schema of the cross section inside the jet and the tip before the pinching.

transition between DC and PF. In order to do so, s, V_o, and V_t have to be estimated as a function of the viscosity of the two fluids and of the applied flow rates. The shape of the jet before the tip obeys to the following rules: the aqueous phase remains in contact with the vertical PDMS wall and the contact angle θ of the truncated jet on the glass is set by the equilibrium conditions. Solving numerically the Stokes equation for a particular flow shape, using the same assumptions as above, a numerical relationship between s and the flow rates is obtained and ajusted using a power law

$$\frac{s}{S_c - s} = A\left(\frac{Q_{water}}{Q_{oil}}\right)^{\alpha}, \qquad (2)$$

where A and α depend on the geometry of the channel and on the viscosity ratio between the two fluids. The estimation of V_o and V_t is trickier since it requires a complete description of the shape of the tip and of the three-dimensional flow. However, assuming that the flow in the tip behaves as a flow in an infinite jet of section S, a link can be expressed between the water flow rate inside the tip $V_t S$ and the oil flow rate around the tip $V_o(S_c - S)$ using Eq. (2) with s equal to S leading to

$$\frac{V_o}{V_t} = B = A^{1/\alpha}\left(\frac{S}{S_c - S}\right)^{1-1/\alpha}. \qquad (3)$$

Keeping in mind that the total flow rate has to be conserved, $Q_{total} = V_t S + V_o(S_c - S)$, V_t and V_o are calculated and introduced in Eq. (1). At the transition $\Omega = 0$ and the ratio $x = Q_{oil}/Q_{water}$ is the solution of

$$\frac{x}{x+1} = \frac{1}{B(S_c - S) + S}\left((B-1)(S_c - S) - \frac{S_c x^{\alpha}}{x^{\alpha} + A}\right). \qquad (4)$$

Figure 7 presents the theoretical flow pattern diagram obtained using Eq. (4). The model predicts a transition between DC and PF. For a given oil flow rate, high water flow rates favor PF. Contrary to capillary numbers arguments, it also describes the effects of viscosity and geometry observed in Fig. 2. Moreover, it is in good agreement with the experimental data without requiring the use of adjustable parameters. The DC-PF transition is calculated taking into account

the geometry of the channel, the viscosity of the phase, and the contact angle θ measured by using confocal microscopy. Clearly, at low flow rates, our model quantitatively predicts the transition and describes the effect of viscosity, geometry, and wetting conditions. A deviation is noticed at high flow rates. Three-dimensionnal flows inside the tip, modification of the contact angle θ at high flow rates, or variation of the shape of the channels due to the high pressures involved may induces this behavior.

In this paper, we have studied the stability of parallel flows. This stability is linked to the confinement of the flow and cannot be described in terms of capillary numbers. The blocking-pinching effect has been modeled. This description offers guidance to control the stability of immiscible flows in microchannels, a necessary step in the design of two-phase flow related devices.

The authors gratefully acknowledge support from the Aquitaine Région. They wish to thank A. Dodge, P. Panizza, and A. Ajdari for valuable discussions and D. Van Effenterre for his help during confocal microscopy experiments.

[1] T. Thorsen, S. J. Maerkl, and S. R. Quake, Science **298**, 580 (2002).
[2] T. Thorsen, R. W. Roberts, F. H. Arnold, and S. R. Quake, Phys. Rev. Lett. **86**, 4163 (2001).
[3] R. Dreyfus, P. Tabeling, and H. Willaime, Phys. Rev. Lett. **90**, 144505 (2003).
[4] T. M. Squires and S. R. Quake, Rev. Mod. Phys. **77**, 977 (2005).
[5] H. Song, J. D. Tice, and R. Ismagilov, Angew. Chem., Int. Ed. **42**, 768 (2003).
[6] B. Zheng, L. S. Roach, and R. F. Ismagilov, J. Am. Chem. Soc. **125**, 11170 (2003).
[7] T. Maruyama, H. Matsushita, J. I. Uchida, F. Kubota, N. Kamiya, and M. Goto, Anal. Chem. **76**, 4495 (2004).
[8] A. Hibara, H. Matsushita, M. Nonaka, M. Tokeshi, and T. Kitamori, J. Am. Chem. Soc. **49**, 14954 (2003).
[9] J. D. Tice, A. D. Lyon, and R. Ismagilov, Anal. Chim. Acta **507**, 73 (2004).
[10] G. I. Taylor, Proc. R. Soc. London **146**, 501 (1934).
[11] D. C. Duffy, J. C. McDonald, O. J. A. Schueller, and G. M. Whitesides, Anal. Chem. **70**, 4974 (1998).
[12] D. R. Link, S. L. Anna, D. A. Weitz, and H. A. Stone, Phys. Rev. Lett. **92**, 054503 (2004).
[13] P. Garstecki, I. Gitlin, W. DiLuzio, E. Kumacheva, H. A. Stone, and G. M. Whitesides, Appl. Phys. Lett. **85**, 2649 (2004).
[14] P. Garstecki, H. A. Stone, and G. M. Whitesides, Phys. Rev. Lett. **94**, 164501 (2005).